Layer-by-Layer Nanoarchitectonics of Electrochemically Active Thin Films Comprised of Radical-containing Polymers

Author Names: Alexandra D. Easley,[1,*] Sayali V. Shaligram,[2] Ian J. Echols,[3] Kevin Nixon,[3] Steven L. Regen,[2] Jodie L. Lutkenhaus[1,3,z,*]

Affiliation(s): [1] Department of Materials Science and Engineering, Texas A&M University, College Station, Texas, United States of America

[2] Department of Chemistry, Lehigh University, Bethlehem, Pennsylvania, United States of America

[3] Artie McFerrin Department of Chemical Engineering, Texas A&M University, College Station, Texas, United States of America

[z]Corresponding Author E-mail Address: jodie.lutkenhaus@tamu.edu
*Electrochemical Society Member

Abstract

Electroactive coatings based on non-conjugated redox-active polymers have increased in popularity with the development of thin film organic batteries. Control over coating deposition, redox-activity, and ion transport are key to improving their energy storage performance. In this work, the synthesis, solution state electrochemical characterization, and layer-by-layer (LbL) assembly of a nitroxide-based polycation and polyanion are presented. Solution state electrochemical characterization indicates that the rate of electron transfer for the nitroxide polyanion is much higher as compared to the nitroxide polycation. LbL thin films of the nitroxide polyanion and nitroxide polycation are assembled, demonstrating linear growth and tunable thickness (28 nm/LP). This work confirms that the ion transport mechanism of the LbL films during the redox reaction is influenced depending on the charge of the terminating layer, where the nitroxide polyanion can participate in self-doping, which leads to a contribution from cation transport. The nitroxide polyanion-terminated film also exhibits a higher capacity and a slightly reduced charge transfer resistance. However, it was also observed that a more pronounced capacity fade occurred for the polyanion-terminated film than the polycation-terminated film. Taken together, this highlights how oppositely charged radical-containing

polyelectrolytes can form electroactive coatings for possible applications in energy storage or sensing.

Introduction

Electroactive coatings (EACs) are thin films that contain redox-active species that undergo reduction and oxidation. EACs are promising for improved device performance in corrosion protection, actuators,[1] organic electronics,[2-3] and energy storage.[4] In recent years, there has been an increased focus on developing EACs for organic energy storage devices, which utilize redox-active polymers as the coating material.[5] There are two main classes of redox-active polymers used in EACs, conjugated polymers (*e.g.,* polyaniline) and non-conjugated polymers (*e.g.*, poly(TEMPO methacrylate), PTMA). The majority of work on EACs has centered on conjugated polymers due to the ease of their synthesis and deposition, but conjugated polymers can be limited in their practical capacity due to incomplete charge transfer and self-discharge.[6] On the other hand, non-conjugated polymers bear near-theoretical capacities and less self-discharge.[7] This is because the redox activity of non-conjugated polymers is based upon the reversible oxidation-reduction of a pendant active group that bears electronic charge locally; in contrast, conjugated polymers accommodate charge in a delocalized fashion.

It is desirable to broaden EACs to include non-conjugated polymers, but literature indicates certain challenges exist. These challenges include dissolution of the active material, diffusion limitations, and low areal loading.[6, 8] One approach demonstrated to prevent the dissolution of PTMA from EACs was the use of surface-initiated polymerization to polymerize PTMA as brushes from a conductive substrate.[9] This method resulted in coatings up to 84 nm thick, however, the authors demonstrated that as thickness was increased there was a decrease in observed galvanostatic charge-discharge capacity.[9] Another method that prevents dissolution and reduces the diffusion limitations in EACs was a PTMA-polystyrene copolymer that underwent self-assembly from solvent annealing.[10] The authors demonstrated that these 80 nm thin films showed stable galvanostatic cycling performance at high current densities (23.7 $\mu A/cm^2$), but exhibited self-discharge at lower current densities.[10] However, both methods can lead to reduced processability of PTMA and a reduced areal loading of the redox-active unit (due to initiators for surface polymerization and comonomers).

Non-conjugated, redox-active PTMA has been investigated in depth for organic energy storage devices due to PTMA's synthetic simplicity and solution processability. However, PTMA and other TEMPO-containing polymers are subject to dissolution during operation, leading to a gradual loss of capacity. To prevent dissolution, previous work investigated TEMPO-containing polymers that bore a non-dissolving unit for >100 nm thick electrodes. For example, Tokue *et al.* demonstrated poly(TEMPO methacrylate -*co*-styrenesulfonyl(trifluoromethanesulfonyl)imide) with both TEMPO-containing repeat units and trifluoromethanesulfonylimide ($TFSI^-$) anion-containing repeat units that exhibited only slight capacity fade during battery operation.[11] In contrast, Aqil *et al.* produced ionic liquid homopolymers with both TEMPO and imidazolium cations; however, these polymers also exhibited some capacity fade after battery operation.[12-13] In our own work, we have addressed dissolution by introducing crosslinkable acrylate units.[14] However, none of these approaches addressed thin film applications, which have different challenges, including substrate adhesion and conformability.

As has been demonstrated for conjugated polymers,[15-20] the layer-by-layer (LbL) assembly technique can produce EACs with controllable thickness, good adhesion, and conformal deposition. In the LbL technique, oppositely charged polymers are alternately deposited onto a surface of interest from aqueous solutions, building up layers of polycations and polyanions in a stepwise fashion.[21-22] The internal structure of the film is often highly interdigitated, but stratified structures can be obtained as well.[23-25] Therefore, oppositely charged polymers that are soluble in water are required for strong electrostatic interactions to increase film stability and prevent polymer dissolution. This requirement presents a challenge for the LbL assembly of many non-conjugated redox active polymers because they are often neutral or insoluble in water. For these reasons, LbL assembly has not been widely investigated for non-conjugated redox active polymers, especially for those with TEMPO units. To the best of our knowledge, there exists only two reports of TEMPO-containing LbL films, where one study investigated an LbL film with a nitroxide-containing polyanion[26] and the other study investigated the use of a nitroxide-containing polycation.[27] However these films utilized a complementary polymer that was not redox active, thus diluting the radicals in the film and, therefore, the electroactivity. As of yet, nitroxide-containing polycations and anions have not yet been assembled together

or evaluated as LbL thin films

Here, we report the synthesis and electrochemical characterization of a TEMPO-based polycation and polyanion that are suitable to LbL assembly to produce EACs consisting entirely of radical-containing polyelectrolytes. First, the solution-state electrochemical behavior of these charged polymers is considered. The rate constants for electron transfer are determined from cyclic voltammetry and chronoamperometry. Then, the oppositely charged polymers are assessed for their ability to form LbL assemblies of tunable thickness and mass. The LbL mass, spectroscopic, and thickness growth profiles are determined using quartz crystal microbalance, UV-Vis spectroscopy, and profilometry, respectively. Last, we evaluate the electrochemical performance of the LbL thin films using cyclic voltammetry and galvanostatic cycling. Overall, these results present an alternative method for producing TEMPO-based macromolecular radical thin films of tunable thickness and good adhesion.

Experimental

Materials. Dimethylammonium chloride, 4-oxo-TEMPO, $Ti(O^iPr)_4$, poly(ethylene-alt-maleic anhydride) (M_w = 100,000 - 500,000 g/mol), 4-amino-TEMPO, anhydrous N,N-dimethylformamide, tetrahydrofuran, ethanol, pyridine, diethyl ether, sodium borohydride, branched polyethyleneimine (bPEI, M_w = 25,000 g/mol, M_n = 10,000 g/mol), and hydrochloric acid (HCl, 37% w/w) were purchased from Sigma-Aldrich and used as received. Poly(4-vinylbenzyl chloride) (PVBC) (M_w = 39,500 g/mol, M_n = 22,500 g/mol was purchased from Polymer Source Inc. and used without further purification. Acetone, methanol, dichloromethane (DCM), and sodium chloride (NaCl) from VWR BDH Chemicals were used without any further purification. Ultrapure water (MQ water) was collected from a Milli-Q® water purification system (18 MΩ·cm). Indium tin oxide (ITO)-coated glass (CUV5B) was purchased from Delta Technologies. Ti/Au quartz crystal microbalance 5 MHz substrates (part # 149257-1) were purchased from MAXTEK and cleaned with 5:1:1 MQ H_2O:ammonium hydroxide:hydrogen peroxide at 75 °C for 5 mins before use.

*Synthesis of the nitroxide polycation (**1**).* The modified TEMPO group, 4-(*N,N*-dimethylamino)-TEMPO, was synthesized as previously described (**Scheme 1**).[28] A solution of poly(4-vinylbenzyl chloride) (PVBC), (0.30 g, 1.96 mmol repeat unit) and 4-(*N,N*-

dimethylamino)-TEMPO (1.184 g, 5.92 mmol) in 8 mL of *N,N*-dimethylformamide was stirred at room temperature for 24 h. The mixture was then poured into 20 mL of diethyl ether to precipitate the polymer, followed by trituration (two times) with 20 mL of diethyl ether to give 500 mg (72%) of **1**. Anal. calcd. For $C_{20}H_{34}ClN_2O_2$ (monohydrate) C, 64.93; H, 9.26; Cl, 9,58; N, 7.57. Found: C, 63.48; H, 9.27; Cl, 8.73; N, 8.14.

*Synthesis of the nitroxide polyanion (**2**).* The polyanion containing a pendant nitroxide group (nitroxide polyanion) was synthesized following a previous report by Lappan *et al* (**Scheme 2**).[29] In summary, a solution was prepared by stirring 0.50 g (3.96 mmol of repeat unit) of poly(ethylene-*alt*-maleic anhydride) in 10 mL of anhydrous pyridine for 3 h at 50°C under an argon atmosphere. To this solution a solution made from 1.71 g (10 mmol) of 4-amino-TEMPO plus 5 mL of anhydrous pyridine was added. The resulting solution was stirred at room temperature for 3 h under an argon atmosphere. The polymer was then isolated by precipitation into 60 mL of *n*-hexane. The polymer was purified by dissolving it in 15 mL of anhydrous pyridine followed by precipitation in 60 mL of *n*-hexane. Subsequent drying under reduced pressure for 24 h at room temperature afforded 1.12 g (94%) of **2**. Anal. calcd. for $C_{15}H_{25}N_2O_4$: C, 60.59; H, 8.47; N, 9.42. Found: C, 58.60; H, 8.90; N, 9.53.

Chemical characterization. All IR spectra were recorded on solid samples using a Thermo Scientific Nicolet iS10 spectrometer in attenuated total reflection (ATR) mode. Elemental analysis was performed by Midwest Microlab. Thermal gravimetric analysis (TGA) was performed on a TA Instruments Q50 with a heating rate of 10 °C/ min from ambient temperature to 900 °C under a nitrogen environment (60 mL/min) to identify the 5% degradation temperature (T_{5d}). Differential scanning calorimetry (DSC) was performed using a Q200 DSC (TA Instruments) with a heat–cool–heat cycle. The samples were ramped from −40 °C to T_{5d} at a rate of 5 °C/min. The glass transition temperature was taken as the inflection point of the second heating cycle.

Preparation and characterization of nitroxide polyanion/nitroxide polycation LbL films. LbL films were prepared on ITO-coated glass, which were cleaned before use by subsequent sonication in soap water, water, DCM, methanol, and acetone. After cleaning, the ITO-coated glass was plasma treated for 10 minutes before immediate submersion into a bPEI solution (0.1 wt% in 0.1 M NaCl in H_2O) for 15 minutes followed by a 2-minute rinse in MQ water to

generate a base layer on the substrate. After the rinse, the nitroxide polyanion/nitroxide polycation LbL films were deposited using an alternating immersion process. The bPEI-coated substrate was first immersed in a nitroxide polyanion solution (15 mM by polymer repeat unit, 0.1 M NaCl, pH 4) for deposition, followed by 2 min, 1 min, and 1 min rinses in 0.1 M NaCl, pH 4 water. After the three rinses, the substrate was submerged in a nitroxide polycation solution (15 mM by polymer repeat unit, 0.1 M NaCl, pH 4) for 15 min, followed by another three rinses. This cycle completed one layer pair. This processes was repeated until the desired number of layer pairs was attained, resulting in bPEI-(nitroxide polyanion/nitroxide polycation)$_n$ films, where n is the number of layer pairs. After assembly, the films were dried at ambient conditions for 24 h. We observed that drying films under vacuum results in the loss of electrochemical activity due to kinetic trapping of the polymer chains.

Film characterization. UV–Vis spectra were collected from 300 nm to 800 nm using a Hitachi U-4100 UV–Vis–NIR spectrophotometer (341-F). Micrographs of the film morphology were collected using optical microscopy (Leica DM4 M) and atomic force microscopy (AFM, Bruker Dimension Icon AFM). Profilometric thickness and root-mean-square (RMS) roughness (R_q) of thin films were measured using a profilometer (KLA Tencor D-100). Quartz crystal microbalance (QCM) (MAXTEK RQCM Research) was used to determine the dry film composition during LbL assembly. The change in frequency was reported after each polymer was deposited and converted to mass using the Sauerbrey equation.

Electrochemical characterization. To confirm the redox behavior of the polymers, solution-state cyclic voltammetry (CV) and chronoamperometry (CA) were used with a three-electrode cell. The working electrode was the LbL film on ITO-coated glass, the counter electrode was platinum wire, and the reference electrode was Ag/AgCl (sat). CV from 0.3 to 1.1 V *vs.* Ag/AgCl for 45 cycles at 50 mV/s was used to determine the polymer's stability. Following the stability cycling, two cycles of CV at 2, 5, 10, 25, 50, and 100 mV/s were conducted, followed by CA with a step from 0.3 to 1.1 V *vs.* Ag/AgCl. The diffusion coefficient of electron transfer (D_{et}) was determined by using the Cottrell equation (**Equation 1**), assuming a semi-infinite condition[30]:

$$i = \frac{nFAC_E}{\sqrt{\pi t}}\sqrt{D_{et}} = \tau\frac{nFAC_E}{\sqrt{\pi}}\sqrt{D_{et}}$$

Equation 1

where *i* is the current output from CA (in mA), *n* is the number of electrons transferred per repeat unit (1 equiv mol^{-1}), *A* is the electrode area (in cm^2), and C_0^* is the total concentration of redox sites (or repeat units in mol/cm^3). With the determined D_{et} values, the apparent electron transfer rate constant ($k_{ex,app}$) was calculated using the Dahms-Ruff equation (**Equation 2**).

$$k_{ex,app} = \frac{6D_{et}}{C_0^* \delta^2}$$

Equation 2

where δ is the average site distance determined from MD simulations (discussed below). Finally, the heterogenous rate constant (k^0) was determined using the method of Nicholson (**Equation 3**) assuming the diffusion coefficient of the oxidized and reduced species are equal to D_{et}.

$$\psi = \frac{k^0}{(\pi D_{et} f v)^{1/2}}$$

Equation 3

where ψ is a dimensionless rate parameter (using the peak separation from 10 mV/s), *v* is the scan rate of CV (in V s^{-1}), and D_{et} is the diffusion of electron transfer from CA (in cm^2/s). Last, $f = F/RT$, where F is Faraday constant (or 96585 C/mol e^-), R is the gas constant (or 8.3124 J/mol K) and T is the temperature (in K).

To study the electrochemical properties of the LbL film, CV, CA, galvanostatic charge-discharge (GCD), and electrochemical impedance spectroscopy (EIS) were conducted in a similar three-electrode cell, but the working electrode was the LbL film of interest assembled on ITO-coated glass. CV from 0.3 to 1.1 V *vs.* Ag/AgCl was used to condition the films for 45 cycles at 50 mV/s. Following conditioning, two cycles of CV (from 0.3 to 1.1 V *vs.* Ag/AgCl) at 2, 5, 10, 25, 50, 100, 200, and 400 mV/s were conducted to determine a scan rate dependence. After CV testing, GCD was carried out for 5 cycles at 2, 5, 10, and 20 $\mu A/cm^2$, followed by 100 cycles at 2 $\mu A/cm^2$. Unless otherwise stated, a Solartron potentiostat (Solartron Electrochemical Interface 1287) was used for all electrochemical testing. EIS was conducted at a potential of 0.8 V *vs.* Ag/AgCl (sat.) with an amplitude of 10 mV in a frequency range of 0.1 to 5×10^6 Hz (10 steps per decade).

Results and Discussion

Synthesis and characterization of the nitroxide polycation and the nitroxide polyanion. The nitroxide polycation (**1**) was synthesized by installation of 4-(N,N-dimethylamino)-TEMPO to poly(4-vinylbenzyl chloride) (PVBC) (**Scheme 1**).[28] 4-(N,N-dimethylamino)-TEMPO was collected from the amination of 4-oxo-TEMPO with dimethylamine hydrochloride, as seen from the appearance of the 1750 cm^{-1} vibration (**Figure S1**). Installation of 4-(N,N-dimethylamino)-TEMPO onto PVBC was confirmed by the appearance of the C-N stretching peaks (**Figure S2**). The resulting nitroxide polycation degree of polymerization and Đ was assumed to match that of the precursor PVBC (M_n ≈ 22.5 kDa and Đ ≈ 1.8) or 44.6 kDa (**Table 1**).

The nitroxide polyanion (**2**) was synthesized by the installation of 4-amino-TEMPO to poly(ethylene-alt-maleic anhydride) (**Scheme 2**). Successful installation of the TEMPO moieties was confirmed by the appearance of the COOH and $CONH_2$ peaks (**Figure S3**). For both the nitroxide polycation and polyanion, an excess of the nitroxide-containing moieties was used to prepare both polymers and the elemental analysis was consistent with a nitroxide being added to virtually all repeat units present.

From thermogravimetric analysis, the 5% decomposition temperature (T_{5d}) for the nitroxide polycation was 55.4 °C, whereas the T_{5d} for the nitroxide polyanion was 66.0 °C (**Figure S4**). From differential scanning calorimetry, the T_g of the nitroxide polycation and the nitroxide polyanion were -26.9 °C and -29.4 °C, respectively. These glass transitions are considerably lower than that of neutral PTMA (*ca.* 170 °C), perhaps because the charge groups on the nitroxide polyelectrolytes may provide extra free volume for faster segmental relaxation.

After confirming the polymer structures, the redox behavior of the polyelectrolytes was characterized using solution-state cyclic voltammetry (CV) and chronoamperometry (CA). From CV, the nitroxide polycation exhibited a redox couple at $E_{1/2}$ = 0.80 V *vs.* Ag/AgCl, whereas the nitroxide polyanion exhibited a redox couple at $E_{1/2}$ = 0.72 V *vs.* Ag/AgCl (**Figure 1a-b**). The nitroxide polycation exhibited a smaller peak separation of 54 mV, compared to 74 mV for the nitroxide polyanion. The difference in peak separation suggests that the redox reaction for the nitroxide polycation is more reversible than the nitroxide polyanion. Additionally, the nitroxide polyanion shows a pronounced shoulder in oxidation and reduction.

This shoulder can be attributed to anion self-doping that occurs during the electrochemical reaction. More specifically, nitroxide-based charged copolymers from Tokue *et al.* and neutral homopolymers from Wang *et al* exhibited similar features.[11, 31] In addition, both the nitroxide polyanion and polycation here exhibited reasonable electrochemical stability with a slight fade in peak oxidation current (~13% fade) over 45 CV cycles for both polyelectrolytes, which could be a result of the nitroxide radical or oxoammonium cation oxidizing amines present in the polymer (**Figure S5**).[32-33] Both polymers showed an increase in peak current with increased scan rate that scaled linearly with the square root of the scan rate, indicative of a diffusion-limited reaction (**Figure 2a-b**).

In addition to CV, chronoamperometry studies were conducted to determine the solution-state electron transfer rate constants for both polymers (**Figure 2c-d**). The linear region of the Cottrell plots allowed for calculation of the diffusion coefficient of electron transfer (D_{et}) (**Table 1**). Once D_{et} was calculated, the apparent electron transfer rate constant ($k_{ex,app}$) and the heterogenous rate constant (k^0) were calculated using the Dahms-Ruff equation and the method of Nicholson, respectively. The nitroxide polyanion exhibited significantly higher D_{et}, $k_{ex,app}$, and k^0 values compared to the nitroxide polycation. This enhanced rate of electron transfer for the nitroxide polyanion could be caused by the negative charge of the pendant group acting as a counter ion and negating the need for anion uptake, as previously hypothesized for bulk TEMPO-containing polymers.[31]

Nitroxide polycation/nitroxide polyanion LbL Films. Following confirmation of the polymers' solution-state electroactivity, LbL assembly of the nitroxide polycation and polyanion was carried out up to 10.5 layer pairs (LPs) (**Figure 3a**), for which the polyanion was the terminating layer. Digital images of the films were taken with varying LPs, and a change in apparent film color with increasing number of LPs was visible (**Figure 3b**). UV-Vis spectroscopy also showed an increase in the peak absorbance for the LbL films at a similar wavelength to that of the nitroxide radical (*ca.* 500 nm) (**Figure 3c**).

To better characterize the surface of the LbL films with different terminating layers (polycation or polyanion), optical microscopy and atomic force microscopy (AFM) were used. From optical microscopy, there was little difference in surface morphology for the differing terminating layers (**Figure 4a-b)**. Similar results were obtained from AFM, which showed that

the surface morphologies of both the 10 and 10.5 LP films were similar with discrete agglomerates on the surface. The 10 LP film, with a polycation terminating layer, had an R_q of 53.1 nm, whereas the 10.5 LP film, with a polyanion terminating layer, had one of 107 nm.

The growth profiles of the LbL films were monitored as a function of LP using UV-Vis absorbance at 500 nm, quartz crystal microbalance (QCM), and profilometry. The absorbance at 500 nm increased with increasing LPs and did not show a significant dependence on terminating layer (**Figure 5a**). The profilometic thickness growth profile showed that the LbL films increased by 28.2 nm per LP (**Figure 5b**). There was an observed increase in thickness and profilometric roughness for the 10.5 LP film with the polyanion terminating layer. Finally, the mass change during layer deposition was monitored with QCM and showed a linear increase of 2.74 ng/cm^2 per LP deposited (**Figure 5c**). From the QCM mass growth profiles, the film composition was determined to be 62.7 ± 17.7 wt% of nitroxide polyanion. The resulting film density was 1.01 g/cm^3.

Electrochemical properties of nitroxide polycation/nitroxide polyanion LbL films. To determine the nature of the redox reaction for the LbL films, CV and galvanostatic cycling were conducted in a 3-electrode beaker cell. From CV, both the 10 and 10.5 LP films exhibited a redox couple at $E_{1/2}$ = 0.65 V *vs.* Ag/AgCl, (**Figure 6a-b**). At 100 mV/s, the 10 LP film exhibited a smaller peak separation of 147 mV, compared to 216 mV for the 10.5 LP film. At low scan rates the 10 LP film shows peak splitting, whereas the 10.5 LP film did not (**Figure 6c**). The observed peak splitting could be attributed to separate cation and anion transport events. Anion transport is suppressed in the 10.5 LP film due to Donnan exclusion of the chloride anion[34] or the reduced mobility of the film from the odd-even effect[35-36] caused by the polyanion terminating layer. The cyclic voltammogram results at 50 mV/s for the 10.5 LP film were compared to previous literature (**Table S1)**. Our film was able to reach a greater thickness, which resulted in a larger peak current compared to other studies using nitroxide-based polyelectrolytes for LbL, indicating the added material led to greater energy storage. As a further control, LbL assembly was also attempted here with the nitroxide polycation and poly(styrene sulfonate) (PSS) polyanion; however, the negatively charged groups of PSS led to overoxidation of the nitroxide groups and prevented any appreciable electrochemical response.[37]

For further discussion, the odd-even effect has been widely studied for polyelectrolyte multilayers.[34-36] Calvo et al. studied LbL films with osmium-modified polycations, in which a shift in redox potential associated with the charge of the terminating layer was observed.[34] Elsewhere, anion uptake was observed for polycation-terminated films and cation exchange for polyanion-terminated films.[34] Similar conclusions were found by Sato et al. who studied ferrocene-modified polycation containing LbL films and observed that the polycation-terminated films exhibited stronger electrochemical responses associated with enhanced anion transport.[36] Additionally, Lappan et al. studied the dynamics of TEMPO-labeled LbL films and found that the polycation-terminated films exhibited higher mobility than those terminated with the polyanion.[35] Taken together, this demonstrates that LbL assemblies can be utilized to manipulate the ion transport mechanism by changing the charge of the terminating layer.

In addition to CV, galvanostatic cycling was also conducted to consider the capacity performance of the LbL films (**Figure 7**). The theoretical capacities of the nitroxide polycation and polyanion are 76 mAh/g and 84 mAh/g, respectively. At the lowest current density (2 $\mu A/cm^2$), the 10.5 LP film exhibited significantly higher capacity (4.8×10^{-4} mAh/cm^2) than the 10 LP film (2.6×10^{-4} mAh/cm^2) (**Figure 7a-b**). However, at current densities > 2 $\mu A/cm^2$, the two films showed similar capacities. In general, the capacities are low, which might be attributed to diffusion limitations, limited accessibility of the TEMPO groups due to the tightly ion-paired LbL film, or the low mass loading (36.5 $\mu g/cm^2$ for 10.5 LP film). In future work, this might be adjusted changing the assembly conditions to promote a more coiled chain conformation (such as added salt) which would produces films that are less dense.

The capacity performance was also considered for a varying number of layer pairs. As the number of LPs increased, there was an increase in capacity (**Figure 7c**). This increase in capacity with LP was particularly notable at low current densities. These films were then cycled for 100 cycles at 2 $\mu A/cm^2$ (**Figure 7d**). With increasing LPs, the capacity increased fairly linearly with respect to layer pair number (**Figure 7e**) and coulombic efficiency also increased. The film with 2 LPs exhibited a poor coulombic efficiency of ~70%, likely because the film was patchy and not well formed in the first few cycles of LbL assembly. For 6 LPs and greater, the Coulombic efficiency was ~100%, which we attribute to the formation of an electrochemically percolating film over the substrate. As for capacity retention, LbL films of 6

and 8 LPs exhibited the best retention, but higher LP films (10 and 10.5) showed more pronounced capacity fade. The reason for this is not immediately clear but may arise from side reactions or irreversible swelling of the film.

Electrochemical impedance spectroscopy (EIS). To evaluate the charge transfer characteristics of the 10 and 10.5 LP films, EIS was used. An equivalent circuit consisting of a solution resistance (R_s), charge transfer resistance (R_{CT}), Warburg diffusion element (W_O), and constant phase element (CPE) (**Figure 8a**) was utilized to represent the electrolyte and LbL thin film. The Nyquist plots for both the 10 and 10.5 LP films exhibited characteristic semi-circle shapes associated with the films' R_{CT} (**Figure 8b**), where the radius was slightly larger for the 10 LP film when compared to the 10.5 LP film. There was little difference between the Bode plots for the 10 and 10.5 LP films (**Figure S7**). **Table 2** presents the parameters from the equivalent circuit model for both films and two control films (only the nitroxide polycation and 2 LP). Specifically, R_{CT} for the 10 LP film was slightly higher than the 10.5 LP film, which we attribute to the lower activation barrier allowed by the polyanion-terminating layer that can participate in self-doping.

Conclusions

In conclusion, the synthesis and solution state electrochemical characterization of a nitroxide-based polycation and polyanion were presented. From solution state electrochemical characterization, it was determined that the nitroxide polyanion's redox reaction is slightly less reversible and exhibits a pronounced shoulder in oxidation and reduction associated with anion self-doping. The nitroxide polyanion also exhibited significantly higher D_{et}, $k_{ex,app}$, and k^0 values compared to the nitroxide polycation. In addition to solution state characterization, the nitroxide polyanion and nitroxide polycation were LbL-assembled to fabricate thin films of tunable thickness (28 nm/LP). QCM and profilometry showed that the growth of the films was linear. The ion transport mechanism of the LbL films during the redox reaction differed depending on the terminating layer, where the nitroxide polyanion can participate in self-doping, which leads to a contribution from cation transport. However, the LbL film with the nitroxide polyanion terminating layer led to an improved capacity at 2 $\mu A/cm^2$. Finally, electrochemical impedance spectroscopy was utilized to study charge transfer within the LbL

films. The nitroxide polyanion terminating layer led to a slightly reduced charge transfer resistance.

Taken together, these films show the promise of nitroxide-containing polyelectrolytes for EACs, but more work is needed to realize their full potential. Looking to the future, further work should be conducted to produce thicker films that are fully electrochemically accessible. The films produced here were 300-400 nm thick, and depositing more layer pairs could, in principle, increase the areal capacity. However, this might manifest in capacity fade during cycle, as we observed for the 10 and 10.5 LP films. To address this, one might consider adding conductive particles during the LbL assembly process to promote electron transfer from the redox-active polymer to the current collector. With future improvements, nitroxide-based polyelectrolytes might provide EACs that are conformal, adherent and functional for applications ranging from energy storage to sensing.

Acknowledgments

A.D.E and J.L.L acknowledge support from grant DE-SC0014006 funded by the US Department of Energy, Office of Science. The Lehigh contribution to this work was supported by the U.S. Department of Energy, Office of Science, Office of Basic Energy Sciences under Award DE-FG0205ER15720. A.D.E. acknowledges support by the National Science Foundation Graduate Research Fellowship under Grant No. DGE:1746932.

References

1. Jun, K.; Kim, J.; Oh, I.-K. *Small* **2018,** *14* (35), 1801603.
2. Wałęsa-Chorab, M.; Skene, W. G. *ACS Applied Materials & Interfaces* **2017,** *9* (25), 21524-21531.
3. Ariga, K.; Lvov, Y.; Decher, G. *Physical Chemistry Chemical Physics* **2022**.
4. Tebyetekerwa, M.; Xu, Z.; Li, W.; Wang, X.; Marriam, I.; Peng, S.; Ramkrishna, S.; Yang, S.; Zhu, M. *ACS Applied Energy Materials* **2018,** *1* (2), 377-386.
5. Gu, M.; Kim, B.-S. *Accounts of Chemical Research* **2021,** *54* (1), 57-69.
6. Rohland, P.; Schröter, E.; Nolte, O.; Newkome, G. R.; Hager, M. D.; Schubert, U. S. *Progress in Polymer Science* **2022,** *125*, 101474.
7. Gerlach, P.; Balducci, A. *Electrochimica Acta* **2021,** *377*, 138070.
8. Wang, S.; Easley, A. D.; Lutkenhaus, J. L. *ACS Macro Letters* **2020,** *9* (3), 358-370.
9. Hung, M.-K.; Wang, Y.-H.; Lin, C.-H.; Lin, H.-C.; Lee, J.-T. *Journal of Materials Chemistry* **2012,** *22* (4), 1570-1577.
10. Hauffman, G.; Vlad, A.; Janoschka, T.; Schubert, U. S.; Gohy, J. F. *Journal of Materials Chemistry A* **2015,** *3* (38), 19575-19581.
11. Tokue, H.; Murata, T.; Agatsuma, H.; Nishide, H.; Oyaizu, K. *Macromolecules* **2017,** *50* (5), 1950-1958.
12. Aqil, M.; Ouhib, F.; Aqil, A.; El Idrissi, A.; Detrembleur, C.; Jérôme, C. *Eur. Polym. J.* **2018,** *106*, 242-248.
13. Aqil, M.; Aqil, A.; Ouhib, F.; El Idrissi, A.; Dahbi, M.; Detrembleur, C.; Jérôme, C. *Eur. Polym. J.* **2021,** *152*, 110453.
14. Wang, S.; Park, A. M. G.; Flouda, P.; Easley, A. D.; Li, F.; Ma, T.; Fuchs, G. D.; Lutkenhaus, J. L. *ChemSusChem* **2020,** *13* (9), 2371-2378.
15. Jeon, J.-W.; O'Neal, J.; Shao, L.; Lutkenhaus, J. L. *ACS Applied Materials & Interfaces* **2013,** *5* (20), 10127-10136.
16. Jeon, J.-W.; Kwon, S. R.; Lutkenhaus, J. L. *Journal of Materials Chemistry A* **2015,** *3* (7), 3757-3767.
17. Yun, J.; Echols, I.; Flouda, P.; Wang, S.; Easley, A.; Zhao, X.; Tan, Z.; Prehn, E.; Zi, G.; Radovic, M.; Green, M. J.; Lutkenhaus, J. L. *ACS Applied Materials & Interfaces* **2019,** *11* (51), 47929-47938.
18. Pandey, M.; Sadakata, S.; Nagamatsu, S.; Pandey, S. S.; Hayase, S.; Takashima, W. *Synthetic Metals* **2017,** *227*, 29-36.
19. Zhang, K.; Hu, Z.; Xu, R.; Jiang, X.-F.; Yip, H.-L.; Huang, F.; Cao, Y. *Advanced Materials* **2015,** *27* (24), 3607-3613.
20. Jang, M.; Kim, S. H.; Lee, H.-K.; Kim, Y.-H.; Yang, H. *Advanced Functional Materials* **2015,** *25* (25), 3833-3839.
21. Li, Y.; Wang, X.; Sun, J. *Chemical Society Reviews* **2012,** *41* (18), 5998-6009.
22. Richardson, J. J.; Cui, J.; Björnmalm, M.; Braunger, J. A.; Ejima, H.; Caruso, F. *Chemical Reviews* **2016,** *116* (23), 14828-14867.
23. Ghostine, R. A.; Jisr, R. M.; Lehaf, A.; Schlenoff, J. B. *Langmuir* **2013,** *29* (37), 11742-11750.
24. Soltwedel, O.; Ivanova, O.; Nestler, P.; Müller, M.; Köhler, R.; Helm, C. A. *Macromolecules* **2010,** *43* (17), 7288-7293.

25. Zahn, R.; Coullerez, G.; Vörös, J.; Zambelli, T. *Journal of Materials Chemistry* **2012,** *22* (22), 11073-11078.
26. Takahashi, S.; Aikawa, Y.; Kudo, T.; Ono, T.; Kashiwagi, Y.; Anzai, J.-i. *Colloid and Polymer Science* **2014,** *292* (3), 771-776.
27. Fu, Q.; Zoudanov, I.; Gustafsson, E.; Yang, D.; Soleymani, L.; Pelton, R. H. *ACS Applied Materials & Interfaces* **2017,** *9* (6), 5622-5628.
28. de Vries, W.; Doerenkamp, C.; Zeng, Z.; de Oliveira, M.; Niehaus, O.; Pöttgen, R.; Studer, A.; Eckert, H. *J. Solid State Chem.* **2016,** *237*, 93-98.
29. Lappan, U.; Wiesner, B.; Zschoche, S.; Scheler, U. *Appl. Magn. Reson.* **2013,** *44* (1), 181-188.
30. Sato, K.; Ichinoi, R.; Mizukami, R.; Serikawa, T.; Sasaki, Y.; Lutkenhaus, J.; Nishide, H.; Oyaizu, K. *Journal of the American Chemical Society* **2018,** *140* (3), 1049-1056.
31. Wang, S.; Li, F.; Easley, A. D.; Lutkenhaus, J. L. *Nature Materials* **2019,** *18* (1), 69-75.
32. Sato, K.; Ono, T.; Sasano, Y.; Sato, F.; Kumano, M.; Yoshida, K.; Dairaku, T.; Iwabuchi, Y.; Kashiwagi, Y. *Catalysts* **2018,** *8* (12).
33. Nelsen, S. F.; Hintz, P. J. *Journal of the American Chemical Society* **1972,** *94* (20), 7114-7117.
34. Calvo, E. J.; Wolosiuk, A. *Journal of the American Chemical Society* **2002,** *124* (28), 8490-8497.
35. Lappan, U.; Rau, C.; Naas, C.; Scheler, U. *Macromolecules* **2019,** *52* (6), 2384-2392.
36. Sato, H.; Anzai, J.-i. *Biomacromolecules* **2006,** *7* (6), 2072-2076.
37. Yu, I.; Jeon, D.; Boudouris, B.; Joo, Y. *Macromolecules* **2020,** *53* (11), 4435-4441.

Scheme 1. Synthetic route for the nitroxide polycation.

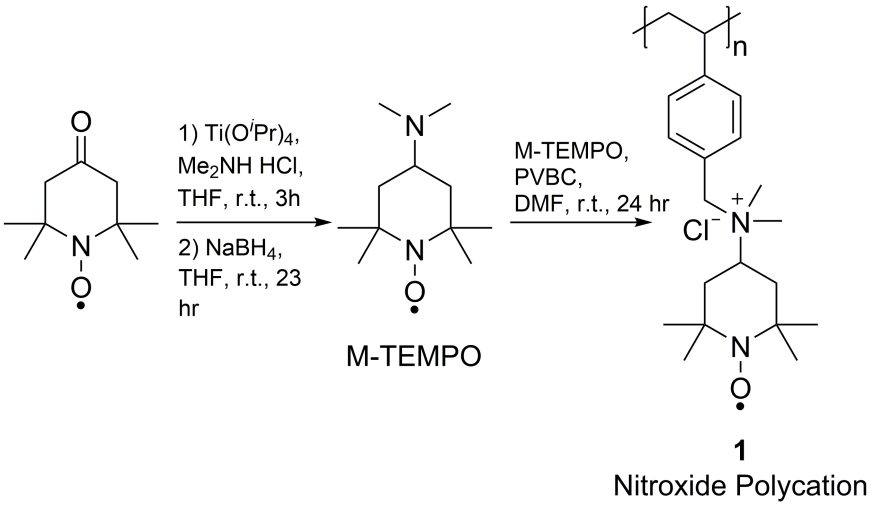

Scheme 2. Synthetic route for the nitroxide polyanion (deprotonated carboxylic acid at pH 4).

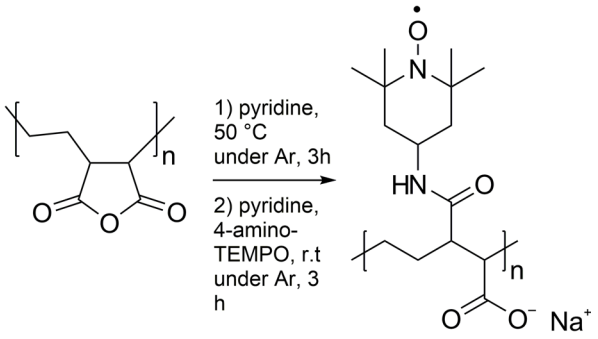

2
Nitroxide Polyanion

Table 1. Polymer and solution-state properties.

Physical property	Nitroxide Polycation (**1**)	Nitroxide Polyanion (**2**)
# of RUs	147[a]	-[b]
M_n or M_w (kDa)	M_n = 44.6	M_w = 100-500[b]
Đ	1.8[a]	-[b]
D_{et} (cm^2/s)	$1.7 \pm 0.3 \times 10^{-6}$	$25.2 \pm 12.3 \times 10^{-6}$
$k_{ex,app}$ (M^{-1} s)	$1.6 \pm 0.2 \times 10^{12}$	$23.6 \pm 11.6 \times 10^{12}$
k^0 (cm/s)	$8.2 \pm 0.6 \times 10^{-3}$	$30.8 \pm 7.8 \times 10^{-3}$

[a] From precursor polymer poly(4-vinylbenzyl chloride).

[b] M_w of the precursor polymer poly(ethylene-alt-maleic anhydride) from the manufacturer is listed. Because of the wide range, Đ and the number of repeat units were not estimated.

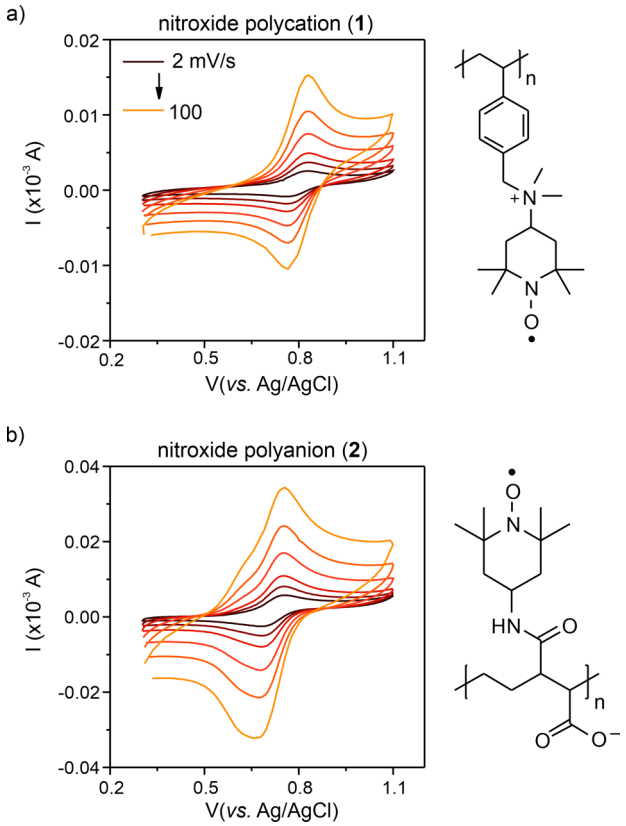

Figure 1. Solution state cyclic voltammograms at varying scan rates for the a) nitroxide polycation and b) nitroxide polyanion. The polymer was dissolved at 1 mM of repeat unit in 0.1 M NaCl aqueous solution. The polymer solution was tested in a three-electrode cell with a glassy carbon working electrode, a platinum wire counter electrode, and a Ag/AgCl (sat.) reference electrode. Legend in panel b) applies to panel a). Polymer structures are shown to the right of their corresponding cyclic voltammograms. A comparison of 2 mV/s for both polymers can be found in **Figure S6**.

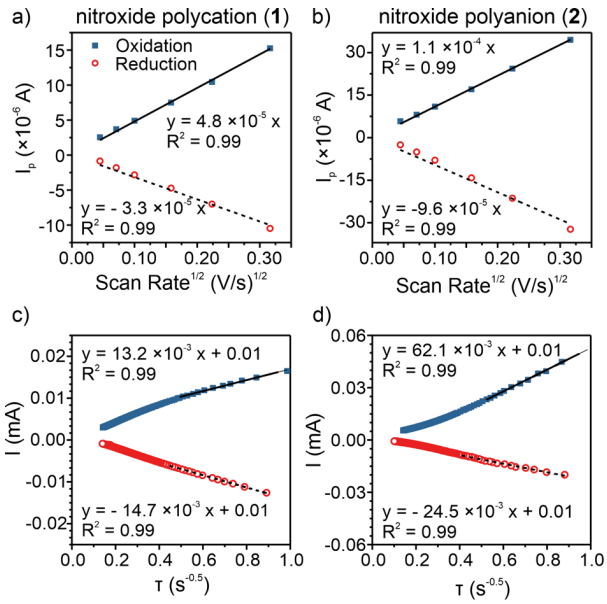

Figure 2. Solution-state peak current *vs*. square root scan rate for the a) nitroxide polycation and b) the nitroxide polyanion from CV. Solution-state Cottrell plots of chronoamperometry data for the c) nitroxide polycation and d) the nitroxide polyanion. The electrolyte solution was 1 mM of the nitroxide repeat unit in 0.1 M NaCl in water with a platinum wire counter electrode, Ag/AgCl (sat.) reference electrode, and a glassy carbon working electrode. Legend in panel a) applies to panels b-d.

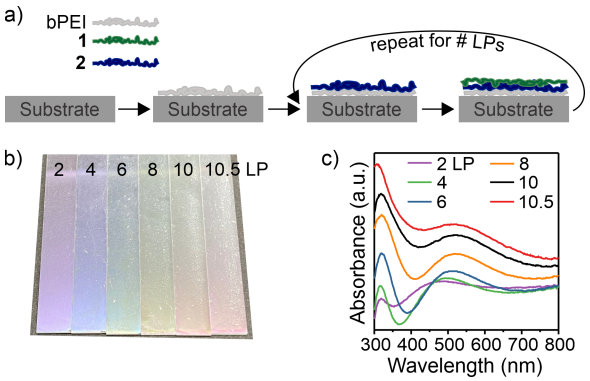

Figure 3. a) LbL assembly process including a branched polyethyleneimine (bPEI) base layer followed by alternating deposition of the nitroxide polyanion (**2**) and polycation (**1**) for the desired number of layer pairs (LPs). b) Digital images of the LbL films with increasing LPs. c) UV-Vis spectra for films with varying number of LPs.

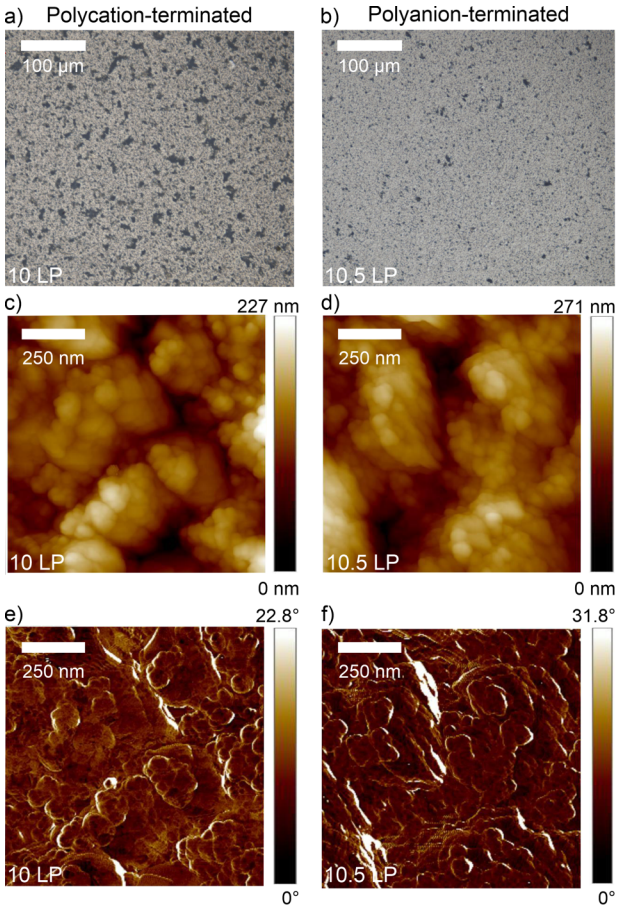

Figure 4. a) Optical micrographs of the 10 LP film and b) 10.5 LP film. AFM micrographs of the c-d) height and e-f) phase for the 10 LP film (c, e) and the 10.5 LP film (d, f). 10 LPs indicated polycation-terminated films and 10.5 LPs indicates polyanion-terminated films.

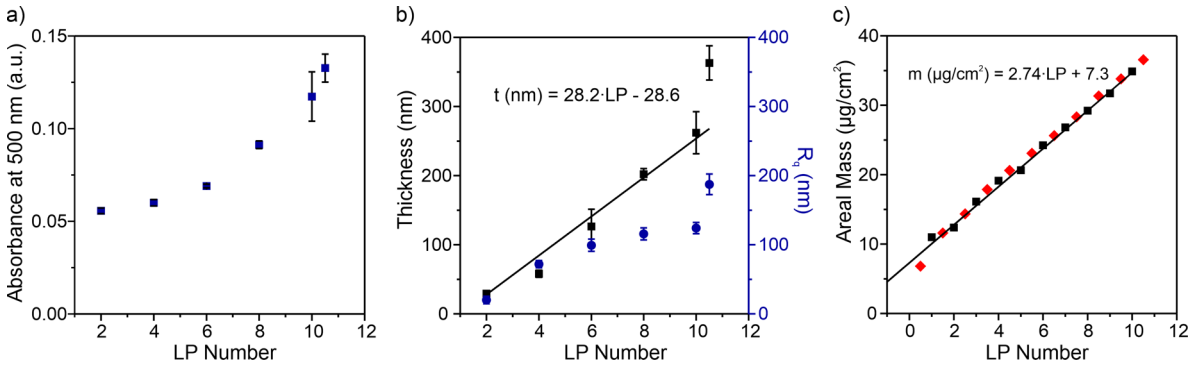

Figure 5. Growth profiles as a function of LP number from a) UV-Vis absorbance at 500 nm, b) profilometric thickness and root mean square roughness (R_q), and c) QCM areal mass deposition. UV-Vis spectra are from **Figure 3c**. In panel c), the red diamonds correspond to polyanion deposition and the black squares to polycation deposition.

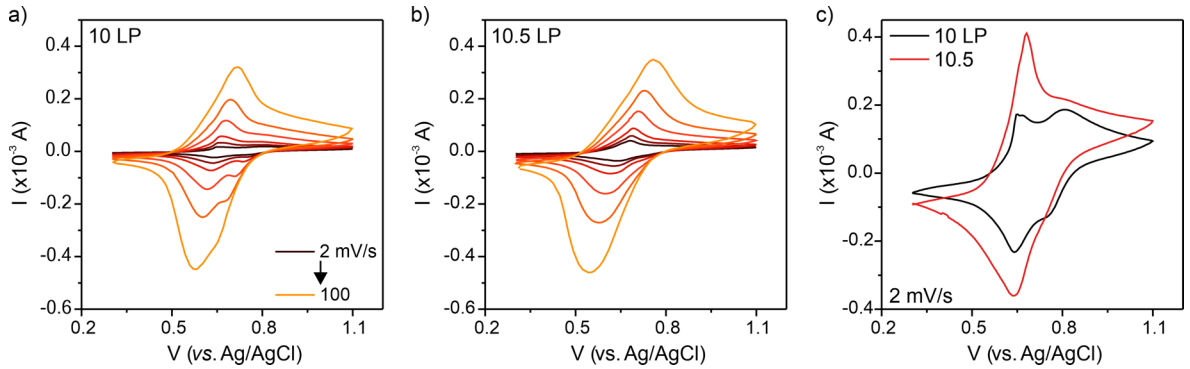

Figure 6. Cyclic voltammograms at various scan rates for a) a 10 LP film and b) a 10.5 LP LbL film consisting of the nitroxide polycation and the nitroxide polyanion. c) Cyclic voltammograms at 2 mV/s for 10 and 10.5 LP. Legend in panel a) applies to panel b).

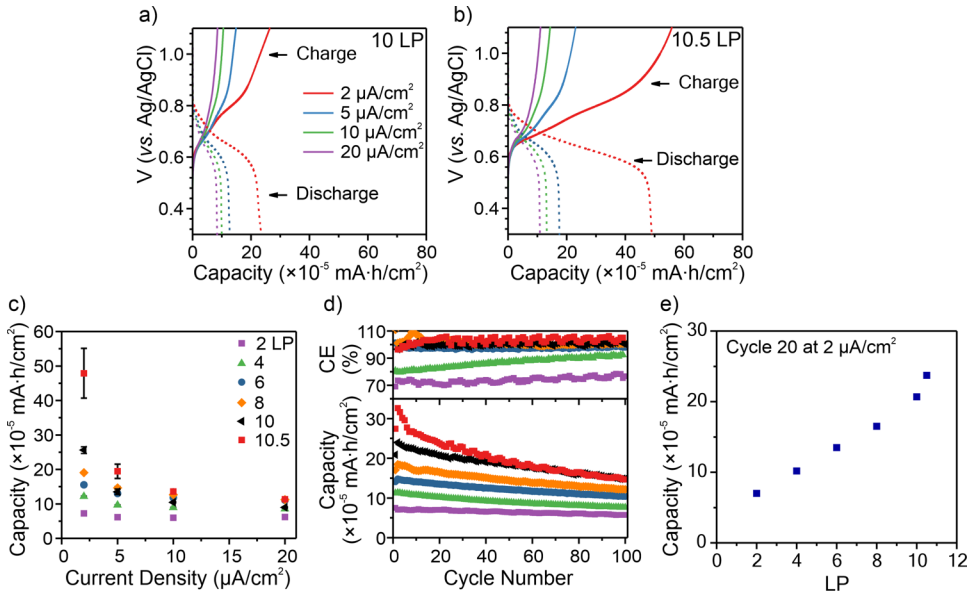

Figure 7. Galvanostatic charge-discharge profiles for a) 10 LP and b) 10.5 LP LbL films consisting of the nitroxide polycation and the nitroxide polyanion. Comparison of c) the rate capability and d) the coulombic efficiency cycling stability for LbL with different LPs. e) Capacity *vs.* LP number for cycle 20 of the galvanostatic charge-discharge at a current density of 2 μA/cm^2 from (d). The legend in (c) also applies to the curves shown in (d).

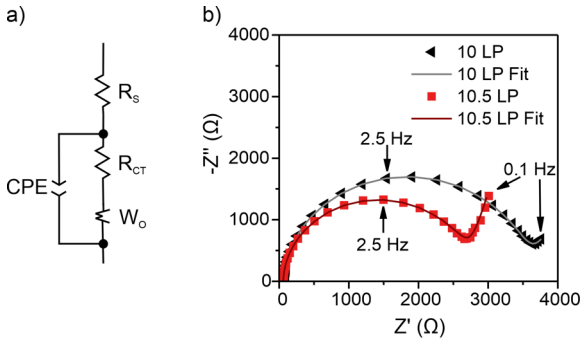

Figure 8. a) The equivalent circuit use to model the to the EIS data. b) Nyquist plots for 10 LP and 10.5 LP with their fit lines. EIS was conducted at a potential of 0.8 V *vs.* Ag/AgCl (sat.) with an amplitude of 10 mV in a frequency range of 5×10^6 Hz to 0.1 Hz (10 steps per decade). Bode plots can be found in **Figure S7**.

Table 2. Equivalent circuit modeling parameters for the 2, 10, and 10.5 LP films. Thin film nitroxide polycation on glassy carbon was used as a control sample. The Nyquist plots for the nitroxide polycation and 2 LP films are found in **Figure S8**.

EIS Fit Parameter	**10 LP (cation-terminated), 262 nm thick**	**10.5 LP (anion-terminated), 362 nm thick**	**Nitroxide Polycation on Glassy Carbon, *ca.* 570 nm thick**	**2 LP (cation-terminated), 29 nm thick**
R_S (Ω)	59 ± 0.1	58 ± 0.1	44 ± 0.1	55 ± 0.1
R_{CT} (Ω)	3519 ± 22	2692 ± 6	6117 ± 62	982 ± 5
W_O	0.36 ± 0.01	0.42 ± 0.01	0.18 ± 0.1	0.45 ± 0.1
CPE (μF)	18 ± 0.1	17 ± 0.1	15 ± 0.1	22 ± 0.1